

Plastic Damage Induced Fracture Behaviors of Dental Ceramic Layer Structures Subjected to Monotonic Load

Raorao Wang, PhD,¹ Chenglin Lu, PhD,² Dwayne Arola, PhD,^{3,4} & Dongsheng Zhang, PhD^{5,6}

¹The Tenth People's Hospital of Tongji University, Shanghai, PR China

²Weigao Orthopaedic Device Co. Ltd., Weihai, Shandong, PRChina

³Department of Mechanical Engineering, University of Maryland Baltimore County, Baltimore, MD

⁴Department of Endodontics, Prosthodontics, and Operative Dentistry, Baltimore College of Dental Surgery, University of Maryland, Baltimore, MD

⁵Department of Mechanics, Shanghai University, Shanghai, PR China

⁶Shanghai Key Laboratory of Mechanics in Energy Engineering, Shanghai, China

Keywords

DIC; fracture; monotonic load; crack; ceramic crowns.

Correspondence

Dongsheng Zhang, Department of Mechanics, Shanghai University, 99 Shangda Rd., Shanghai, 200444, PR China. E-mail: donzhang@staff.shu.edu.cn

Research supported by NSFC grant #11172161; the Shanghai Leading Academic Discipline Project #S30106; the Innovation Program of Shanghai Municipal Education Commission #12ZZ092; the State Key Laboratory of Oral Diseases (Sichuan University) Grant SKLODSCU2009KF03; the Science and Technology Commission of Shanghai Municipality grants #11195820900 and #10ZR1423400. The investigation was also supported in part by grant R01-DE016904 (PI: Dwayne D. Arola) from the National Institutes of Dental and Craniofacial Research.

The authors deny any conflicts of interest.

Accepted December 3, 2012

doi: 10.1111/jopr.12035

All-ceramic crowns have become increasingly popular due to their improved esthetics and biocompatibility in comparison to traditional metal-ceramic restorations.^{1,2} They are, however, brittle and prone to tensile failure. The main fracture modes of all-ceramic dental crowns include chipping^{3,4} of veneering porcelain and bulk fracture of supported core. Bulk fracture is a catastrophic failure, which immediately leads to loss of load-bearing capacity of the restoration.⁵

Great efforts have been devoted to improving the flexural strength of core ceramics to increase the fracture resistance of all-ceramic restorations. As fracture strengths have progres-

Abstract

Purpose: The aim of this study was to compare failure modes and fracture strength of ceramic structures using a combination of experimental and numerical methods.

Materials and Methods: Twelve specimens with flat layer structures were fabricated from two types of ceramic systems (IPS e.max ceram/e.max press-CP and Vita VM9/Lava zirconia-VZ) and subjected to monotonic load to fracture with a tungsten carbide sphere. Digital image correlation (DIC) and fractography technology were used to analyze fracture behaviors of specimens. Numerical simulation was also applied to analyze the stress distribution in these two types of dental ceramics.

Results: Quasi-plastic damage occurred beneath the indenter in porcelain in all cases. In general, the fracture strength of VZ specimens was greater than that of CP specimens. The crack initiation loads of VZ and CP were determined as 958 ± 50 N and 724 ± 36 N, respectively. Cracks were induced by plastic damage and were subsequently driven by tensile stress at the elastic/plastic boundary and extended downward toward to the veneer/core interface from the observation of DIC at the specimen surface. Cracks penetrated into e.max press core, which led to a serious bulk fracture in CP crowns, while in VZ specimens, cracks were deflected and extended along the porcelain/zirconia core interface without penetration into the zirconia core. The rupture loads for VZ and CP ceramics were determined as 1150 ± 170 N and 857 ± 66 N, respectively.

Conclusions: Quasi-plastic deformation (damage) is responsible for crack initiation within porcelain in both types of crowns. Due to the intrinsic mechanical properties, the fracture behaviors of these two types of ceramics are different. The zirconia core with high strength and high elastic modulus has better resistance to fracture than the e.max core.

sively increased from Empress II glass ceramic (320 MPa) to alumina (550 MPa), and to Y-TZP (1450 MPa),⁶ more studies have focused on fatigue performance of all-ceramic crowns.^{7,8} Nevertheless, a single posterior restored crown, composed of a weak porcelain layer and a strong core layer, can be subjected to high load due to parafunctional activity. Although the duration of the force is short, the magnitude could reach more than 1000 N, especially for clenching and bruxism forces, potentially leading to catastrophic failure of the restoration.⁹ Therefore, it is necessary to understand the fundamental failure mechanism of all-ceramic dental crowns subjected to

monotonic load. To study the fracture behavior by Hertzian contact testing, all-ceramic crowns composed of veneering porcelain and supported core are usually simplified into flat layer structures due to complex geometry of their dental occlusal surface.^{6,10-12} This methodology, using the tungsten carbide spheres with similar cuspal radius to applied contact loads at the flat ceramic plate, has been widely accepted in the analysis and characterization of fracture and deformation properties of dental ceramics.¹³⁻¹⁵ Three primary damage modes include surface cone cracks driven by tensile stress, a subsurface quasi-plastic zone driven by shear stress, and radial cracks driven by tensile stress.^{12,16} Cone and radial cracks are typically fracture modes for brittle materials, while quasi-plasticity is manifest as a residual surface impression in ceramics and resembles plastic metallic materials.¹³ Due to the opacity of dental ceramics, no effective experimental methods measure real-time displacements, crack initiation, and growth while loading.¹⁷ As such, some unique methods were introduced to identify the deformation and failure modes of restored all-ceramic crowns. For instance, all-ceramic crowns were sectioned from the indentation sites to observe cone cracks after loading.^{16,18} Fractography has also been considered as an effective method to find the crack origin and growth path in glass-like materials.^{19,20} As this technique is a post analysis method on fragments, it cannot be used to track the crack growth while loading. Previous studies have shown that digital image correlation (DIC) could be used to identify deformation and crack growth in sliced tooth-like specimens,¹⁷ compare strain distributions within the surrounding bone of implant-supported crowns,²¹ and measure the dehydration shrinkage of dental materials^{22,23} and polymerization shrinkage of light-cured dental composites.²⁴ The combination of these two methods could help our understanding of the fracture mechanism of dental materials.

Zirconia and IPS e.max hot-pressed dental ceramics are widely used in China. A previous study reported that the fracture strength of zirconia ceramics, regardless of the brand (Cercon Smart, Lava, Procera, and CEREC 3) could reach more than 1000 N.²⁵ To understand the fracture mechanism in the prevailing dental ceramic structures, this study sought to investigate the fracture behaviors of veneered e.max Press and a selected zirconia dental ceramic. Sliced layer structures were prepared and subjected to monotonic load to fracture. DIC and fractographic analysis were adopted to identify the location of crack initiation and evaluate the nature of crack extension. Finite element modeling (FEM) was applied to evaluate the mechanics associated with contact loading and the potential failure modes.

Materials and methods

Specimen fabrication

Two types of all-ceramic systems, hot-pressed lithium-disilicate glass ceramic (IPS e.max Press, Ivoclar-Vivadent, Schaan, Liechtenstein) and yttria-stabilized zirconia polycrystal ceramic (Lava, 3M ESPE, Seefeld, Germany) were selected. The flat veneer/core bilayered specimens were designed as shown in Figure 1. This layout has proved effective in monitoring crack initiation and evolution to fracture in the layers during loading.¹⁷

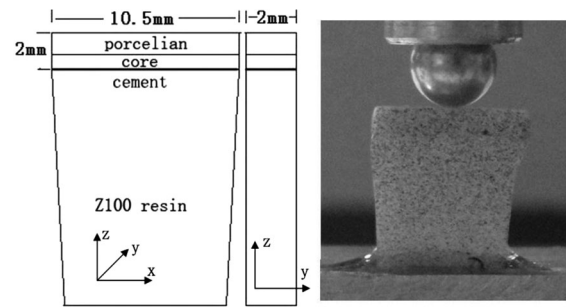


Figure 1 Dimensions of flat layer specimen.

The flat veneer/core bilayered dental ceramics were made according to the size of a standard first right mandibular molar (D50-500A, Nissin Dental Products Co., Ltd., Kyoto, Japan), and the two types of all-ceramic crowns were fabricated according to the specially designed procedures. A 2-mm thick slice was sectioned from the bilayered ceramic plate with a diamond wheel. For the hot-press e.max material, the sectioned crowns were placed back into the furnace to remove possible microcracks potentially introduced during sectioning and sanding, and then glued onto the dental polymeric substrate. The 0.8-mm thick e.max core was veneered with 1.2-mm thick porcelain (IPS e.max Ceram, Ivoclar-Vivadent), for a total thickness of 2.0 mm above the substrate. The lower surface of the e.max core was etched with 4.5% hydrofluoric acid for 20 seconds, rinsed with distilled water, silanized, and cemented to the composite resin (Z100, 3M ESPE, St. Paul, MN) aged for 2 weeks with a dual-cure resin cement (RelyX-ARC, 3M ESPE). For the zirconia dental restoration, a 1.4-mm thick porcelain (Vita VM9, Vita Zahnfabrik, Bad Sackingen, Germany) was veneered onto the 0.6 mm zirconia core. The lower surface of the zirconia core was roughened with 600-grit silicon carbide paper and cemented (RelyX-ARC) to the Z100 composite resin. Six specimens were prepared for each type of dental ceramic. All specimens were immersed in distilled water at 37°C for 72 hours prior to testing.

Considering the limited number of specimens in each group, a statistical power analysis was conducted to assess if the sample size was large enough to illustrate the load differences in crack initiation and fracture between the two types of all-ceramic crowns under compressive loads. In the analysis, the probability of committing a Type I error, false positive, was set as $\alpha = 0.05$. The probability, β , of committing a Type II error, false negative, was calculated from the experimental results. The statistical power is accordingly determined as $1 - \beta$. The power analysis from the experimental results revealed a sample size of 6 each was sufficient to demonstrate a difference at $\alpha = 0.05$.

Monotonic load to fracture

To facilitate the application of DIC, the normal surface of the sliced specimens (the x-z plane in Fig 1) was sprayed with a thin coating of splashed fine black speckles.²⁶ The specimens were subjected to monotonic load to fracture at the center of the porcelain surface through a tungsten carbide sphere with a diameter of 6 mm. The contact load was applied using a

Zwick BZ2.5/TS1S universal test machine at a 0.05 mm/min rate (displacement control mode). A video camera (JAI CV-A1) was placed perpendicular to the sliced specimen surface to acquire sequential speckle images necessary for performing DIC. According to the image resolution (1376×1035 pixels), one pixel length represented approximately $10 \mu\text{m}$. Sequential images were acquired at a constant frequency of 2 Hz during loading. The documented crack initiation loads and fracture loads for each group of specimens were analyzed using one-way ANOVA with significance defined as $p \leq 0.05$.

DIC and fractographic analysis

DIC is a noncontact optical method for full-field displacement and strain measurement, requiring digital images captured before and after deformation.^{26,27} The displacement distribution within the specimens was examined as a function of loading and visualized in the direction of loading (vertical direction) by transforming the magnitude of the displacement components to gray scales.¹⁷ As DIC provides a displacement resolution in 0.01 subpixels (i.e., approximately $0.1 \mu\text{m}$) by using a combination of subpixel technique and Newton–Raphson iteration algorithm,²⁸ it provides an accurate detector to indicate how the crack initiated and propagated with the increase of load. Since the displacement distribution is not continuous across the edge of the crack, a crack can be identified by a pronounced discontinuity in the grayscale map.¹⁷ Fractographic analysis can be used to analyze the location of the flaw origin and cause of crack initiation in failed brittle components according to fracture markings.²⁰ In this study, the fractured surfaces of the failed parts of specimens were analyzed using SEM (JSM-6700F, JEOL, Tokyo, Japan) to search for key failure features providing evidence of the crack initiation and propagation direction with comparison to the results of DIC.

Finite element modeling

For the case of purely elastic contact with a hard spherical indenter on flat ceramics, the contact radius is given by¹³

$$a^3 = \frac{3PR}{4E_{\text{eff}}} \quad (1)$$

In the above equation, $\frac{1}{E_{\text{eff}}} = \frac{1-\nu_1^2}{E_1} + \frac{1-\nu_2^2}{E_2}$, where E_1 , E_2 and ν_1 , ν_2 are Young's moduli and Poisson's ratios of the porcelain and the tungsten carbide sphere, respectively. P is the force applied by the indenter whose radius is R . The mechanical properties of the materials are listed in Table 1.²⁹⁻³⁶ In practice, the tungsten carbide spherical indenter could be considered as the rigid sphere, as it is almost 10 times harder and stiffer than the porcelain. Based on the mean monotonic load to fracture from experiments, P was set at 1000 N in the numerical model. In this case, the radius of the contact zone could be calculated from equation (1) as 0.322 mm ($E_1 = 64 \text{ GPa}$ and $\nu_1 = 0.23$) if the radius of the sphere R is 3.0 mm. As the radius of the contact zone is much smaller than the thickness (2.0 mm) of the sliced specimen in the y direction, a 3D axisymmetric model was employed. The 4-node bilinear axisymmetric quadrilateral elements in ABAQUS/Standard (SIMULIA, Providence, RI) were adopted in the meshing procedure.

Table 1 Material properties

Materials	Young's modulus/ E (MPa)	Poisson's ratio	Yield stress Y (MPa)
IPS e.max Ceram ²⁹	64,000	0.23	2109
IPS e.max Press ³⁰	91,000	0.23	
Vita VM9 ^{31,32}	62,250	0.2	2193
Zirconia ³³	210,000	0.3	
RelyX ARC ³⁴	5900	0.27	
Z100 ³⁵	16,600	0.3	
Tungsten carbide sphere ³⁶	612,000		

In the numerical model, the tungsten carbide spherical indenter was considered as the rigid body in a manner of frictionless contact with the flat porcelain surface. To verify if the finite element mesh meets the requirement of convergence, the radius of the contact zone under elastic assumption was compared with the theoretical calculation from equation (1). It was found that a fine element mesh with $10 \times 10 \mu\text{m}$ size around the contact region could result in a radius of 0.320 mm if a linear elastic model was adopted. This value is a good approximation of the theoretical solution (0.322 mm).

To evaluate the elastic–plastic mechanical behavior of the dental ceramics under contact loading, the ideal elastic–plastic constitutive relationship of the ceramics was adopted. Although a strain-hardening coefficient could be obtained using a combination of indentation stress–strain curves and FEM analysis,³⁷ herein, only the yield stress, Y , of the porcelain was estimated according to contact-induced quasi-plasticity,¹³

$$Y = \left(\frac{16P_Y E_{\text{eff}}^2}{9R^2 (1.1\pi)^3} \right)^{1/3} \quad (2)$$

where P_Y is a critical load at yield. In practice, the contact yield load P_Y was determined from observing the deformation field using DIC with the increase of contact load. For ceramic materials, the distribution of elastic deformation is uniform, and the magnitude of deformation is trivial, while the quasi-plastic deformation is usually appreciable and would cause a regionally abrupt change in a global deformation map.

This property can be used to identify if the quasi-plastic deformation occurs from the displacement field resulting from DIC, if the sampling rate of the sequential image is fast enough with respect to the loading rate. In practice, the test machine was set in a displacement control mode with 0.05 mm/min, and the sequential images were recorded at 30 frame/min. Sequential images were subjected to post-DIC analysis with the reference image acquired at unloading state. Once the sequential number of the image, in which the plastic deformation is observed, is retrieved, the corresponding load would be determined as the critical load that causes the ceramic to yield. With the use of equation (2), the yield stress Y can be calculated from the yield load P_Y . This parameter provides evidence to generate the elastic–plastic constitutive behavior of ceramics and will be used in the ideal elastic–plastic numerical modeling.

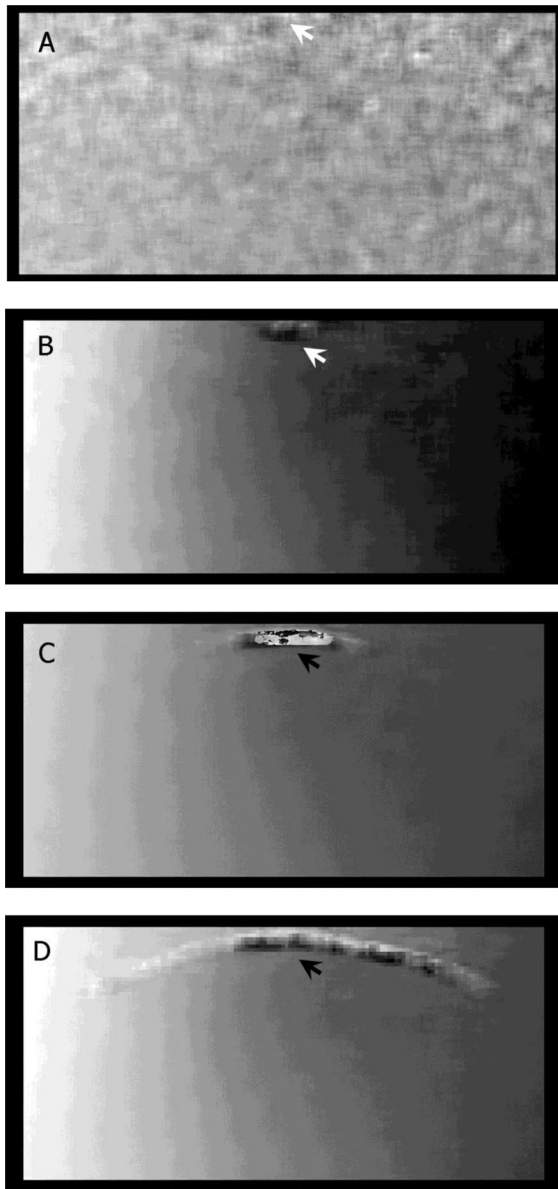


Figure 2 Crack evolution in the e.max structure. Note that the loads corresponding to A, B, C, and D were 420 N, 460 N, 740 N, and 830 N, respectively, and the grayscale was proportional to the displacement components in the vertical direction. The white arrows indicate deformation transferred from elastic to plastic (A and B), and the black arrows indicate crack extension (C and D).

Results

The sequential speckle images acquired during loading were analyzed with commercial DIC software (Matfolt Co., Ltd., Shanghai China). The grayscale distribution, which represented the displacement component in the vertical direction, was used to identify the yield stress of the material, crack initiation, and growth until fracture. The crack growth history in the e.max structures under the quasi-static load is shown in Figure 2. An apparent displacement discontinuity from Figure 2A to Figure 2B can be observed. This was evidence that the porcelain behaved from elastic to plastic. This quasi-plastic zone was located beneath the indenter in the veneer layer (Fig 2B). The critical load causing the plastic deformation was then determined through an averaging process in this group and estimated with the mean value \pm the standard deviation, that is, $P_r = 520 \pm 83$ N. Substituting this number in equation (2), the yield stress for IPS e.max Ceram was determined as 2.1 ± 1.1 GPa. Cracks initiated in the plastic zone boundary inside the veneer other than at the veneer surface and propagated downward in the form of a semicircular path and penetrated into the core ceramic with increasing load (Figs 2C, 2D). Rupture occurred due to fracture of the core layer induced by a radial crack or extension of a curved crack into the core (Fig 3). In all experiments for CP specimens, no debonding between the porcelain veneer and core ceramics was observed.

The crack growth history in zirconia structures (VZ) are shown in Figure 4. Similarly, a quasi-plastic zone was detected through the DIC analysis beneath the indenter in Vita VM9 (Fig 4A). The critical load causing the plastic deformation in Vita VM9 was determined through an averaging process in the VZ group and represented the mean value \pm the standard deviation, that is, $P_r = 630 \pm 76$ N. Substituting this number in equation (2), the yield stress for Vita VM9 was determined as 2.2 ± 1.1 GPa. The curved crack also propagated downward along an arc path until it reached the veneer and core interface (Fig 4B). With the increase of force, the crack extended laterally along the interface instead of penetrating into the core material (Fig 4C). Eventually, debonding at the interface of the zirconia core and veneer caused the load-bearing capacity loss of the specimen (Fig 3B). In all experiments, zirconia cores remained intact. Two types of sliced specimens were sectioned again at the midway of the thickness. With an optical microscope, it was clear that the crack penetrated into the e.max core, while the crack redirected at the interface of the zirconia core and veneer (Fig 5).

Since the CP specimens were fractured in multiple pieces of fragment, only a fractured VZ specimen was observed under the SEM photomicrograph to compare with DIC results. The

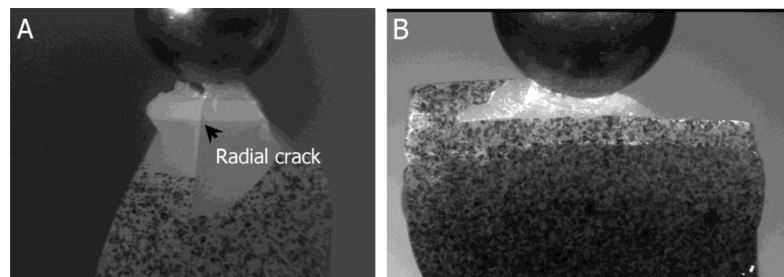


Figure 3 Failed specimens of two types of dental ceramics. (A) CP specimen, (B) VZ specimen.

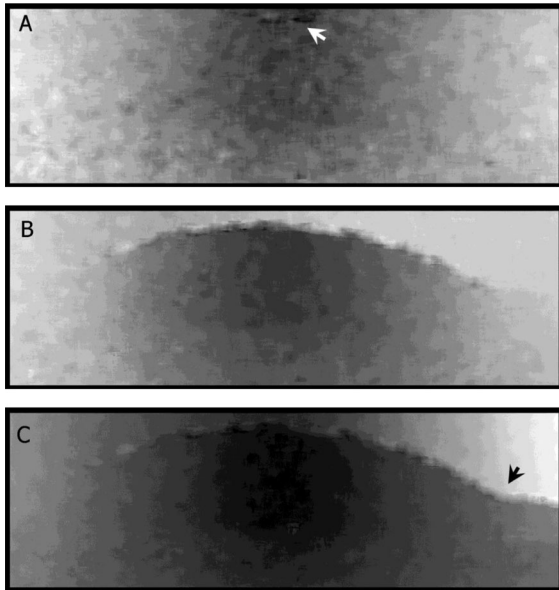


Figure 4 Crack evolution in the zirconia structure. White arrow indicates yield zone (A: P = 612 N). With an increasing load, crack occurred at the yield zone boundary and extended in a semicircular path (B: P = 940 N). Black arrow indicates delamination between porcelain and core interface (C: P = 1000).

surface features of the fractured surface in four regions were analyzed (Fig 6A). In the A1 region, wake hackles indicated the direction of the crack growth (Fig 6A1) was in accordance with DIC results; however, due to the plastic damage right below the contact, it was difficult to distinguish crack origin. It was surprising to find that crack in the veneer not only propagated downward but also extended upward (Fig 6A2). This was consistent with what was reported by Jung *et al*³⁸ in the glass-ceramic, filled with polymer bilayer structure. The crack redirected at the core/veneer interface. Delamination was found at the lateral side of the interface (Fig 6A3), while no crack was observed in the medial side (Fig 6A4). This agreed with what resulted from DIC analysis.

When two types of dental ceramics were subjected to monotonic contact load, the surface deformation was monitored with DIC. Two types of critical loads were defined in the experiments. One is the critical load when the crack was initiated in the specimen, and the other is the ultimate load when the specimen was fractured. Obviously these critical loads could be determined with DIC. The magnitudes of contact loads for

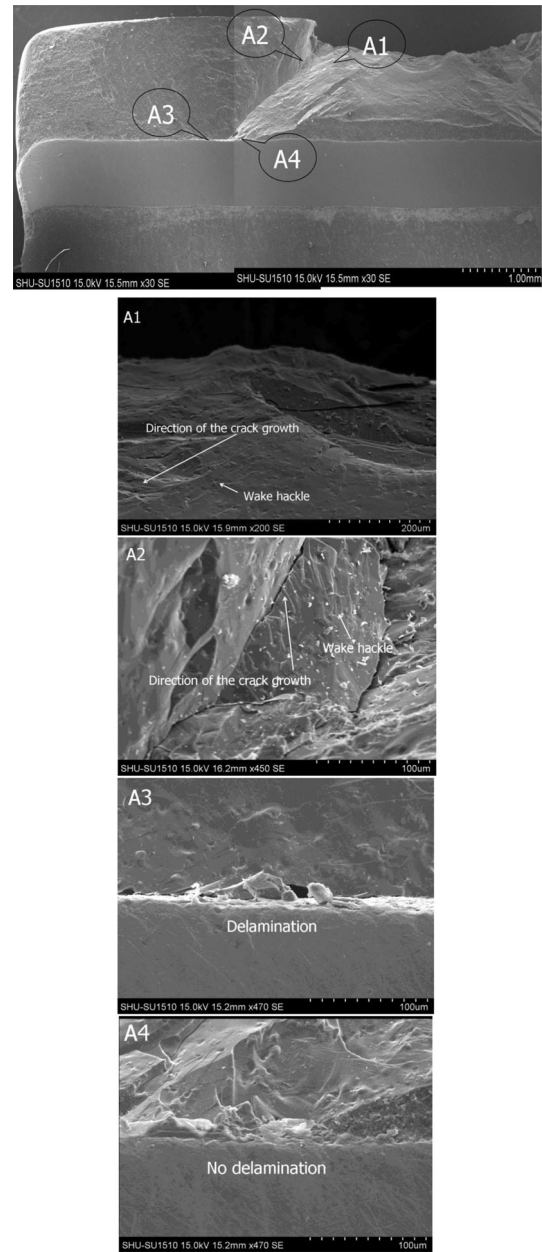


Figure 6 SEM photomicrograph of the fractured zirconia specimen.

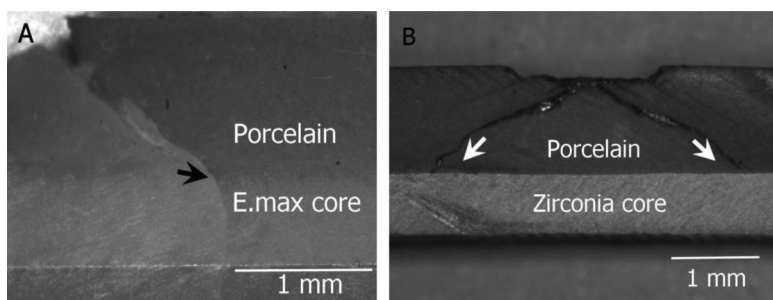


Figure 5 Crack path in the sectioned surface under light microscope. Specimens were sectioned through the contact site. The black arrow indicates the crack penetrated the core layer. The white arrows indicate the crack reached the interface of zirconia core/veneer interface without penetration.

Table 2 Critical contact loads of specimens and statistical analysis ($\alpha = 0.05$)

Specimens		1	2	3	4	5	6	Average (SD)	<i>p</i>	1- β
Crack initiation (N)	CP	698	738	684	783	736	705	724 (36)	0.000	100%
	VZ	1029	918	922	955	1008	913	958 (50)		
Rupture (N)	CP	788	860	858	981	825	830	857 (66)	0.003	98.90%
	VZ	1344	954	1232	1133	1289	945	1150 (170)		

crack initiation and rupture of two types of ceramics were listed in Table 2. From the statistic power analysis, $1 - \beta$ is greater than 0.8, indicating the sample size is adequate, and experimental results are reliable. The magnitudes of crack initiation and rupture loads for VZ structures were approximately 200 N larger than those for CP structures ($p < 0.05$).

FEA results showed that two types of structures had the same form of stress distribution with different stress magnitudes. The distribution of the tresca stress, the maximum principal stress, and the equivalent plastic strain of CP structure is shown in Figure 7. The maximum equivalent plastic strain was observed at subsurface in the veneer (Fig 7C), consistent with experimental results that yield zone occurred beneath contact. When the plastic strain reached a certain value, plastic damage resulted in the formation of cracks (Fig 2B) according to the theory of damage mechanics for plastic materials. Once the crack was formed, it was driven by tensile stress (Fig 7B) to propagate. The observed crack propagation path (Fig 5) in the veneer was in accordance with the trajectory of tensile stress.

Discussion

In the present study, fracture behaviors of two ceramic systems were examined using a combination of experimental and numerical methods. Using sliced flat specimens, DIC was adopted to measure the deformation of the sliced surface. Occurrence of plastic strain, crack initiation, and growth path were identified through the presence of discontinuities in the processed displacement fields. Fractographic analysis verified the DIC results according to the apparent fracture markings of failed specimens. Both of these methods are effective ways to understand crack evolution and fracture behavior of dental ceramics. DIC is a full-field optical method. It could measure displacement/strain components in any direction. As illustrated in this study, it was applied to identify plastic deformation and crack path on the sectioned surface; however, this technique can only be applied on the planar surface. The 2-mm thick sliced dental ceramic specimen was specially designed to facilitate the use of the DIC. In Figures 2 and 4, cracks grow along an arc path toward the veneer/core interface; however, in Figure 5 the crack path right below the contact site is conic. This conflict is due to the geometry of the specimen. Cone cracks would occur in all directions if the layer ceramic structure was subjected to a normal contact load.¹³ As the contact load was applied at the middle of the sliced specimen in this study, what DIC told us is actually the cone crack intersected with the plane, 1 mm away from the contact center where the load was applied. The

intersection of the cone crack and the surface plane revealed an arc path representing the crack growth on the outer sliced surface. To eliminate this difference of crack path, the specimen must be made as thin as possible. On the other hand, ceramic crowns are a 3D structure in the clinical oral environment. The crack growth in a thin 2D structure is not equivalent to that in a true 3D condition. With the selection of 2 mm thickness of the slice, the theoretical and numerical analysis indicated that the contact zone radius was almost the same as 0.32 mm when the specimen was stressed with a tungsten carbide sphere with a 6 mm diameter. From this point of view, the design of the 2-mm thick sliced specimen can also reflect the stress condition of a 3D crown to some extent.

With the use of DIC, this study proposed an effective way to determine the yield stress of the ceramics. Since the plastic deformation takes place regionally, and the magnitude is greater than the uniform elastic deformation, displacement distribution resulting from DIC analysis is helpful to distinguish the sequential image number in which image plastic deformation is found. The yield stress could be estimated by substituting the corresponding yield load into equation (2). The contact yield pressure of Vita VM9 was tested and reported as near 7 GPa with nanoindentation.³¹ According to the relationship that the corresponding yield stress is about one third of contact pressure,³⁹ the yield stress of such material is estimated roughly about 2.3 GPa. The yield stress resulting from this study (2.2 GPa) is in accordance with the relevant studies.

In two types of dental ceramic specimens, quasi-plastic deformation was observed beneath the contact within the veneering porcelain. With the increase of load, the crack was initiated inside the veneer. Contact-induced quasi-plastic deformation was previously discovered in the bonded half blocks of ceramics.^{18,40} A bulk ceramic cube was pre-sectioned into two half blocks and then glued together with adhesion prior to Hertzian contact. From the section view of two half blocks, the plastic deformation zone extended downward and outward without macroscopic cracks, owing to a shear-driven mechanism like that in metals. But at a microscale, it was produced by localized interfacial sliding faults rather than in dislocation slip.^{14,37} The appearance of a yield zone beneath the contact redistributed and reduced the tensile stress near the contact, and reduced the chance for cone cracks initiating from the outside surface.³⁷ With the use of the ideal elastic-plastic mechanical constitutive relationship, the accumulated equivalent plastic strain at the subsurface could cause plastic damage and ductile fracture (Fig 7). This is responsible for the occurrence of cracks with the increase of contact load. This

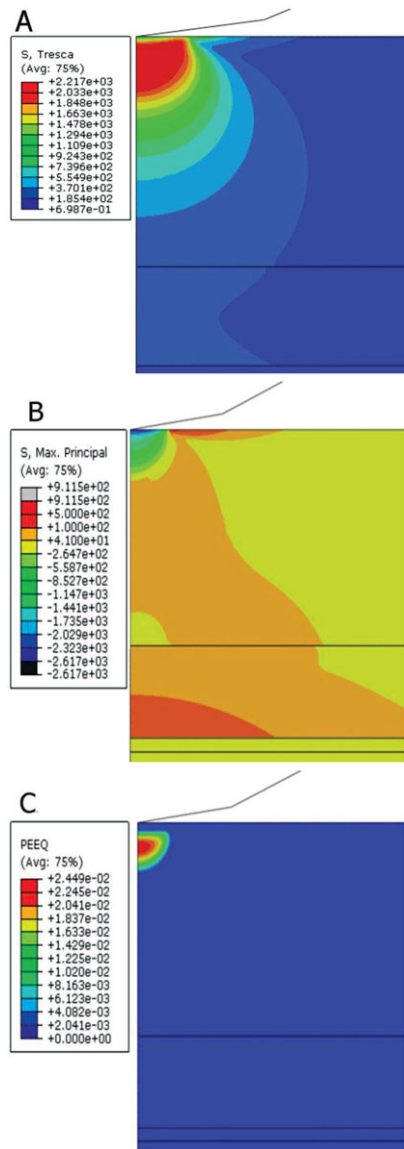


Figure 7 FEA results: The distribution of the tresca stress (A), the maximum principal stress (B), and the equivalent plastic strain. Note that tresca stress is defined as twice the maximum shear stress or the difference between the maximum and minimum principal stresses.

finding that the crack origin was located in the subsurface was also observed in the veneer material (Vita VM7).⁴¹ Subsurface-accumulated, damage-suppressed surface cone cracks may be beneficial for clinical application, because the growth rate of the cone crack could be accelerated by hydraulic pumping as a result of water entrapment in the crack tip from the restoration surface.⁴²⁻⁴⁴

Cone cracks propagated downward in the veneer with increasing contact load (Figs 2B, 4B). While cracks extended to the core/veneer interface, they displayed completely different growth modes in two types of ceramic structures. Crack deflection at the veneer/zirconia framework interface resulted in the delamination of the veneer layer before the complete frac-

ture, while cracks penetrated into the core at the veneer/e.max Press framework interface and caused bulk failure. Cracks are unlikely to propagate from a low-modulus, low-toughness ceramic to a high-modulus ceramic, high-toughness ceramic by Vickers indentation.⁴⁵ While in the present study, cracks propagated from the veneer ($E = 64$ GPa, $K_{IC} = 0.7\sim 0.9$ MPam^{1/2}) into e.max core ($E = 91$ GPa, $K_{IC} = 2.5$ MPam^{1/2}),²⁵ in contrast, cracks deflected along the veneer ($E = 62.25$ GPa, $K_{IC} = 0.7\sim 0.9$ MPam^{1/2})/zirconia core ($E = 210$ GPa, $K_{IC} = 6.5$ MPam^{1/2})⁴⁶ interface, indicating that the ratio of elastic moduli and the fracture toughness of the ceramic system could be important parameters for evaluation of the mechanical quality of dental ceramics.

The mechanical properties of the framework not only affected failure modes but also affected the load-bearing capacity in the two types of ceramic structures. Although the two veneer materials have almost the same yield strength (Table 1) and flexural strength (100 MPa for Vita VM9,⁴⁷ 90 MPa for e.max Ceram⁴⁸), the magnitude of the crack initiation load for Vita VM9 was approximately 200 N larger than that for e.max. A previous study demonstrated that a hard core could decrease the stress within the weak veneer material by all-ceramic fixed partial dentures.⁴⁰ This requires the core itself to be strong and tough to resist possible damage. From the numerical simulation (Fig 7), the tensile stress in the zirconia framework (305 MPa) was larger than that in the e.max Press framework (165 MPa) at the same 1000 N load. High tensile stress distributed at the core bottom is prone to cause bulk fracture of the layer structure. Thus, relatively low-strength e.max core (400 MPa)⁴⁹ is vulnerable to the radial crack compared with high-strength zirconia core (985 MPa).⁵⁰ The zirconia core is strong enough to meet the needs of oral functions,⁵¹ especially parafunctional activities. From this analysis, it is reasonably concluded that high-strength zirconia ceramic system is more suitable for molar restorations, which are normally subjected to large biting forces. Despite the pigment difference between the high-strength zirconia and native enamel, the veneer is sometimes not necessary for the restoration. This could be an alternative to avoid chipping of the veneer. Due to the esthetic concerns and low strength, e.max ceramic system is more suitable for incisor and premolar restorations.

Conclusions

The plastic damage induced fracture behaviors of two types of dental ceramic systems, e.max and zirconia, were studied in this article. The 2-mm thick sliced specimens were subjected to monotonic loads to fracture. DIC and fractography technology were used to analyze plastic deformation, crack origin, and growth path. Numerical simulation with the ideal elastic-plastic constitutive behavior was applied to analyze the intrinsic fracture mechanism of these two types of dental ceramics. The plastic zone was clearly observed with the use of DIC, and the yield stress of the two types of all-ceramic crowns were determined (i.e., 2.1 GPa and 2.2 GPa for IPS e.max Ceram and Vita VM9, respectively). It was found that the plastic damage initiated cracks within the veneer under the contact zone. Cracks penetrated into the e.max core while deflected at the zirconia core/veneer interface. The VZ structure had higher

load-bearing capacity than the CP structure does. The zirconia core with high strength and high elastic modulus has better resistance to fracture than e.max core.

References

- Anusavice KJ: Degradability of dental ceramics. *Adv Dent Res* 1992;6:82-89
- Rekow D, Zhang Y, Thompson V: Can material properties predict survival of all-ceramic posterior crowns? *Compend Contin Educ Dent* 2007;28:362-368
- Quinn JB, Sundar V, Parry EE, et al: Comparison of edge chipping resistance of PFM and veneered zirconia specimens. *Dent Mater* 2010;26:13-20
- Ereifej N, Silikas N, Watts DC: Edge strength of indirect restorative materials. *J Dent* 2009;37:799-806
- Heintze SD, Albrecht T, Cavalleri A, et al: A new method to test the fracture probability of all-ceramic crowns with a dual-axis chewing simulator. *Dent Mater* 2011;27:e10-19
- Kohorst P, Dittmer MP, Borchers L, et al: Influence of cyclic fatigue in water on the load-bearing capacity of dental bridges made of zirconia. *Acta Biomater* 2008;4:1440-1444
- Kelly JR: Clinically relevant approach to failure testing of all-ceramic restorations. *J Prosthet Dent* 1999;81:652-661
- Deng Y, Lawn BR, Lloyd IK: Characterization of damage modes in dental ceramic bilayer structures. *J Biomed Mater Res* 2002;63:137-145
- Ferrario VF, Sforza C, Zanotti G, et al: Maximal bite forces in healthy young adults as predicted by surface electromyography. *J Dent* 2004;32:451-457
- Hermann I, Bhowmick S, Lawn BR: Role of core support material in veneer failure of brittle layer structures. *J Biomed Mater Res B Appl Biomater* 2007;82:115-121
- Hermann I, Bhowmick S, Zhang Y, et al: Competing fracture modes in brittle materials subject to concentrated cyclic loading in liquid environments: trilayer structures. *J Mater Res* 2006;21:512-521
- Lawn BR, Pajares A, Zhang Y, et al: Materials design in the performance of all-ceramic crowns. *Biomaterials* 2004;25:2885-2892
- Lawn BR: Indentation of ceramics with spheres: a century after Hertz. *J Am Ceram Soc* 1998;81:1977-1994
- Peterson IM, Pajares A, Lawn BR, et al: Mechanical characterization of dental ceramic by Hertzian contacts. *J Dent Res* 1998;77:589-602
- Sornsuwan T, Swain MV: Influence of occlusal geometry on ceramic crown fracture; role of cusp angle and fissure radius. *J Mech Behav Biomed Mater* 2011;4:1057-1066
- Lawn BR, Deng Y, Thompson VP: Use of contact testing in the characterization and design of all-ceramic crown like layer structures: a review. *J Prosthet Dent* 2001;86:495-510
- Zhang D, Lu C, Zhang X, et al: Contact fracture of full-ceramic crown Subjected to occlusal Loads. *J Biomech* 2008;41:2995-3001
- Guiberteau F, Padture NP, Lawn BR: Effect of grain size on Hertzian contact in alumina. *J Am Ceram Soc* 1994;77:1825-1831
- Lohbauer U, Amberger G, Quinn GD, et al: Fractographic analysis of a dental zirconia framework: a case study on design issues. *J Mech Behav Biomed* 2010;3:623-629
- Quinn GD: *Fractography of Ceramics and Glasses*. Special Publication 960-16. Washington, DC, Natl Inst Stand Technol, 2007
- Tiozzi R, Lin L, Conrad HJ, et al: A digital image correlation analysis on the influence of crown material in implant-supported prostheses on bone strain distribution. *J Prosthodont Res* 2012;56:25-31
- Zhang D, Mao S, Lu C, et al: Dehydration and the dynamic dimensional changes within dentin and enamel. *Dent Mater* 2009;25:937-945
- Wang R, Mao S, Romberg E, et al: Importance of aging to dehydration shrinkage of human dentin. *Appl Math Mech Engl Ed* 2012;33:1-12
- Li J, Li H, Fok AS, et al: Multiple correlations of material parameters of light-cured dental composites. *Dent Mater* 2009;25:829-836
- Wang R, Wang D, Xu Y, et al: Comparison of compressive strength and fracture mode between four kinds of CAD/CAM zirconia. *J Med Biomech* 2011;26:432-435
- Zhang D, Arola D: Applications of digital image correlation to biological tissues. *J Biomed Opt* 2004;9:691-699
- Tong W: An evaluation of digital image correlation criteria for strain mapping applications. *Strain* 2005;41:167-175
- Schreier HW, Sutton MA: Systematic errors in digital image correlation caused by intensity interpolation. *Opt Eng* 2000;39:2915-2921
- Isgro G, Addisio O, Fleming GJP: Transient and residual stresses induced during the sintering of two dentin ceramics. *Dent Mater* 2011;27:379-385
- Albakry M, Guzzato M, Swain MV: Fracture toughness and hardness evaluation of three pressable all-ceramic dental materials. *J Dent* 2003;31:181-188
- He LH, Swain MV: Nanoindentation derived stress-strain properties of dental materials. *Dent Mater* 2007;23:814-821
- Swain MV: Unstable cracking (chipping) of veneering porcelain on all-ceramic dental crowns and fixed partial dentures. *Acta Biomater* 2009;5:1668-1677
- Yilmaz H, Nemli SK, Aydin C, et al: Effect of fatigue on biaxial flexural strength of bilayered porcelain/zirconia (Y-TZP) dental ceramics. *Dent Mater* 2011;27:786-795
- Aboushelib MN, Jager ND, Kleverlaan CJ, et al: Effect of loading method on the fracture mechanics of two layered all-ceramic restorative systems. *Dent Mater* 2007;23:952-959
- Emami N, Soderholm KM, Berglund LA: Effect of light power density variations on bulk curing properties of dental composites. *J Dent* 2003;31:189-196
- Lawn BR, Deng Y, Miranda P, et al: Overview: damage in brittle layer structures from concentrated loads. *J Mater Res* 2002;17:3019-3036
- Fischer-Cripps AC, Lawn BR: Stress analysis of contact deformation in quasi-plastic ceramics. *J Am Ceram Soc* 1996;79:2609-2618
- Jung YG, Wuttiphan A, Peterson IM, et al: Damage modes in dental layer structures. *J Dent Res* 1999;78:887-897
- Tabor D: *Hardness of Metals*. Oxford, Clarendon Press, 1951
- Cai H, Stevens Kalceff MA, Lawn BR: Deformation and fracture of mica-containing glass-ceramics in Hertzian contacts. *J Mater Res* 1994;9:762-770
- Studart AR, Filser F, Kocher P, et al: Mechanical and fracture behavior of veneer-framework composites for all-ceramic dental bridges. *Dent Mater* 2007;23:115-123

42. Chai H, Lawn BR: Hydraulically pumped cone fracture in brittle solids. *Acta Mater* 2005;53:4237-4244
43. Zhang Y, Song JK, Lawn BR: Deep penetrating conical cracks in brittle layers from hydraulic cyclic contact. *J Biomed Mater Res B Appl Biomater* 2005;73:186-193
44. Kim JW, Kim JH, Thompson VP, et al: Sliding contact fatigue damage in layered ceramic structures. *J Dent Res* 2007;86:1046-1050
45. Kim JW, Bhowmick S, Hermann I, et al: Transverse fracture of brittle bilayers: relevance to failure of all-ceramic dental crowns. *J Biomed Mater Res B Appl Biomater* 2006;9:58-65
46. Fisher H, Waindich A, Telle R: Influence of preparation of ceramic SEVNB specimens on fracture toughness testing results. *Dent Mater* 2008;24:618-622
47. Vita VM9 working instructions, Vita Zahnfabrik, Bad Sackingen, Germany, 2007
48. IPS e.max Ceram scientific documentation. Schaan, Liechtenstein, Ivoclar Vivadent, 2007
49. IPS e.max Press scientific documentation. Schaan, Liechtenstein, Ivoclar Vivadent, 2007
50. Borchers L, Stiesch M, Bach FW, et al: Influence of hydrothermal and mechanical conditions on the strength of zirconia. *Acta Biomater* 2010;6:4547-4552
51. Ortorp A, Kihl ML, Carlsson GE: A 5-year retrospective study of survival of zirconia single crowns fitted in a private clinical setting. *J Dent* 2012;40:527-530

Copyright of Journal of Prosthodontics is the property of Wiley-Blackwell and its content may not be copied or emailed to multiple sites or posted to a listserv without the copyright holder's express written permission. However, users may print, download, or email articles for individual use.